THE JOURNAL OF PHYSICAL CHEMISTRY B

ARTICLE

pubs.acs.org/JPCB

Diversified Nanoparticle Assembly Pathways: Materials Architecture Control Beyond the Amphiphilicity Paradigm

Xin Shu, Zhiqiang Lu, Guangzhao Li, Yuan Tian, Sijing Xia, Xin Zhou, Bin Yang, Heng Shen, Baoqing Liu, and Jin Zhu*

Department of Polymer Science and Engineering, School of Chemistry and Chemical Engineering, State Key Laboratory of Coordination Chemistry, Nanjing National Laboratory of Microstructures, Nanjing University, Nanjing 210093, China

Supporting Information

ABSTRACT: The functional versatility of a chemical system is ultimately dictated by the availability of distinctly accessible architectures. The generation of a diverse array of assembled constructs from a single type of nanoscale building block is a promising yet largely elusive goal. We report herein the utility of a monolayer-modified nanoparticle for the creation of a broad range of architectures. The versatile modes of assembly complement the conventionally used, amphiphilicity-driven strategy. We demonstrate that one can vary the nanoparticle assembly pathways within the confines of solvent media through the modulation of interactions and partitioning of nanoparticles. Merging of the molecular-scale design and higher-ordered arrangement enables diversified assembly through the manipulation of experimental parameters such as solvent, pH, affinity molecule, and temperature. Microfluidics provides an effective channel to control the monodispersity and size on all the architectures attainable in the bulk solution phase. These observations could be further explored for an understanding of diversified matter organization and order generation beyond the amphiphilicity paradigm.

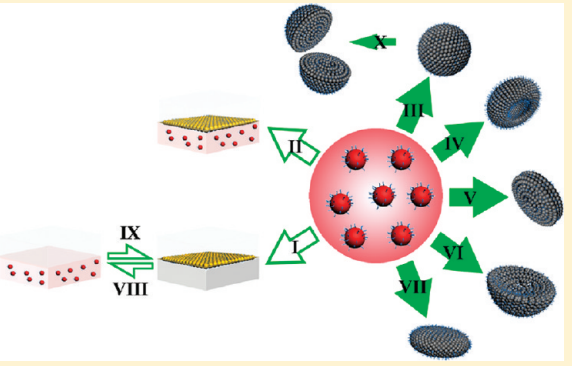

Self-assembly has recently emerged as a promising strategy for the fabrication of sophisticated architectures.[1,2] In principle, one could tailor the properties of target systems through the spontaneous organization of judiciously selected building blocks into desired ensemble constructs.[3] Tremendous efforts have been therefore devoted to the exploration of nanoscale forces for the development of various assembly schemes.[4] Proper arrangement of designer molecular components surrounding the nanoscale objects constitutes the key to the precise engineering of the requisite forces.[4,5] In this regard, monolayer-modified nanoparticles (MMNPs) impart synthetic control over interaction patterns through the tightly bound ligand shell.[6] The translation of uniquely structured MMNPs into higher-ordered constructs requires, ideally, sufficient dynamic freedom to enable the efficient achievement of equilibrium. Fluid phase[7] provides such a permissive environment that allows one to synthesize a rich set of complex architectures. However, the modulation of MMNP surface chemistry for each individual system is required for the fabrication of a particular construct. Indeed, the course of the MMNP assembly process in the fluid phase is strongly dictated by the interaction of MMNPs with their environment. Therefore, in spite of extensive investigations, the question as to how one can generate a diverse array of assembled constructs from a single type of MMNP building block remains largely unaddressed. The diversification of assembly pathways has thus far been achieved primarily through the amphiphilicity framework, where spatial segregation of dissimilar chemical blocks under different environmental conditions leads to the formation of polymorphic structures.[8] Herein, we report on the utility of a carefully designed MMNP for the creation of a broad range of architectures. We demonstrate that one can vary the MMNP assembly pathways within the confines of solvent media through the modulation of interactions and partitioning of MMNPs. These observations could be further explored for an understanding of diversified matter organization and order generation beyond the amphiphilicity paradigm.

RESULTS AND DISCUSSION

1. Structural Considerations for MMNPs. The proof-of-concept MMNP system we devised consists of a gold NP (AuNP) core and a thiol-containing organic shell ($HS(CH_2CH_2O)_4CH_2$-COOH, **1**).[6,9] Linked to the thiol group are a flexible oligo(ethylene glycol) (OEG) unit and a carboxylic acid end-cap. The selection of an MMNP system with molecule **1** as the shell layer is based on the following considerations: (1) The OEG unit is nonionic with affinity toward intriguingly divergent chemical structures, thereby imparting

Received: October 30, 2011
Published: November 03, 2011

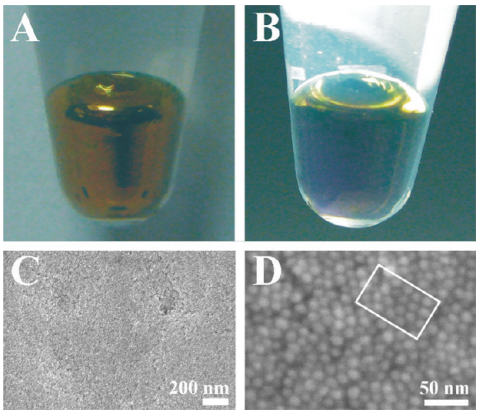

Figure 1. Formation of **1**-MMNP film at the interface of water and ethyl ether. (A) Macroscopic reflectance and (B) macroscopic transmittance images of **1**-MMNP thin film generated by mixing 60 μL aqueous solution of 13 nm **1**-MMNPs and 1 mL ethyl ether. (C, D) SEM micrographs at different magnifications of **1**-MMNP thin film formed on a silicon wafer. The **1**-MMNP thin film was generated by rolling the fluid-phase film over a silicon wafer. The extensively structured, densely packed architecture, at least on the micrometer scale, could be clearly observed. The white box in D indicates the presence of local order in the densely packed film.

distinct MMNP solubility characteristics in varied solvent systems; (2) the carboxylic acid group can be switched between the neutral and the ionic form through the control of pH, thereby enabling regulation over MMNP interactions; and (3) the collective organization of large amounts of molecule **1** on the MMNP surface would confer solvation properties different than individual molecules[10] and could therefore significantly alter their behavior at the fluid-phase boundary. Indeed, the set of phenomena identified herein points toward the importance of merging molecular-scale design and higher-ordered arrangement for the generation of novel nano- and mesoscale structures.

2. Preparation of MMNPs and Confirmation of Ligand Modification. Ligand modification of AuNPs with **1** was accomplished by either the incubation of as-prepared AuNPs (e.g., 13 nm, citrate-stabilized AuNPs) and **1** or the in-situ formation of AuNPs in the presence of **1** (e.g., 4.4 nm AuNPs), affording aqueous-dispersed **1**-MMNPs. The broad synthetic scope allows for the fabrication of MMNPs with a vast range of AuNP core sizes. The successful modification of AuNPs with molecule **1** was confirmed with matrix-assisted laser desorption/ionization time-of-flight mass spectrometry (MALDI-TOF MS) (Figure S1 of the Supporting Information) and was manifested in the high stability of **1**-MMNPs against environmental variables (e.g., heating) as compared to as-prepared AuNPs.

3. Self-Assembly of MMNPs at Liquid−Liquid Interfaces. We started the investigation of the assembly behavior of **1**-MMNPs in a mixture solvent system where the constituent solvents are in the phase separation regime. Interestingly, when ethyl ether was added to the aqueous dispersion of **1**-MMNPs, with the assistance of shaking, spontaneous transfer of **1**-MMNPs to the water/ether interface was observed (Figure 1). The golden reflectance and blue transmittance outlook reflects the close-packing-derived plasmonic coupling of **1**-MMNPs (Figure 1A, B).[7d] The formation of layered structure was confirmed with scanning electron microscopy (SEM) (Figure 1C, D). The deposition of particles at liquid−liquid interfaces has been observed

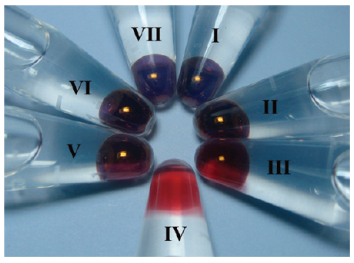

Figure 2. Reversible formation of **1**-MMNP thin film at the liquid−liquid interface through the control of pH. Macroscopic images of a solution containing 60 μL aqueous solution of $^1/_8$-diluted 13 nm **1**-MMNPs and 1 mL ethyl ether (**I**) and after the successive addition of 0.75 μL aqueous solution of 5 mM NaOH (**II**−**IV**). Macroscopic images of the solution after the successive addition of 0.75 μL aqueous solution of 5 mM HCl into the solution from **IV** (**V**−**VII**). The pH value for samples **I**, **II**, **III**, **IV**, **V**, **VI**, and **VII** was measured to be 5.71, 9.14, 9.57, 9.73, 9.34, 7.58, and 6.43, respectively. The percentage of **1**-MMNPs in the bulk aqueous phase for samples **I**, **II**, **III**, **IV**, **V**, **VI**, and **VII** was determined to be 0 (not detectable), 40, 56, 60, 56, 31, and 0% (not detectable), respectively.

by other groups. Surface energies have been used to account for the self-assembly behavior of particles.[11] A decrease in the interfacial energy with the adsorption of particles provides the driving force for their placement at the interface. The confinement energy is dependent on the liquid−liquid contact angle measured on the particle surface, and the particle is most robustly held at the interface when the contact angle equals 90°.[7c,11] The contact angle measurement provides support for the interface-residing capability of **1**-MMNPs (ether/water/**1**-MMNP contact angle: 89°). The bulk aqueous portion is deprived of **1**-MMNPs as evidenced by elemental analysis with inductively coupled plasma atomic emission spectrometry (ICP-AES).

3.1. Stimuli-Responsive Behavior and Chain-End Dependence of Interfacial Assembly. Remarkably, as expected from the pH dependent ionization of carboxylic acid, **1**-MMNPs can be switched between the interfacially confined and aqueous-dispersed state through the adjustment of pH (Figure 2). A control experiment carried out with the pure aqueous solution ruled out pH induced alteration of **1**-MMNP dispersion stability in such a phase. This stimuli-responsive property in the water/ether system reflects both the electrostatic repulsion between and the loss of hydrogen-bonding capability from the deprotonated carboxylic acid. Notably, the assembly behavior of **1**-MMNPs can be further altered when the pH value of the aqueous phase is substantially lower than the pK_a (3.98) of molecule **1** (Figure S2 of the Supporting Information). The suppression of carboxylic acid ionization at pH 2 further strengthens the hydrogen bonding between **1**-MMNPs and renders the assembly structure precipitated out of the solution. The importance of the hydrogen bonding for the interfacial assembly of MMNPs is further demonstrated by the distinctly different behaviors of MMNPs with a hydroxyl ($[S(CH_2CH_2O)_5CH_2CH_2OH]_2$, **2**) and a bromo ($[S(CH_2CH_2O)_4C(O)CH(CH_3)Br]_2$, **3**) end-cap. Thus, although **2**-MMNPs form a golden film at the water/ether interface, a substantial portion of **2**-MMNPs stays in water, rendering the internal part of the dispersion red-colored in appearance. The contact angle measurement hints at the less degree of interfacial confinement for **2**-MMNPs (water/ether/**2**-MMNP contact angle: 85°) as compared to **1**-MMNPs in these solvent media. As expected, no thin film could be identified at the

liquid−liquid interface for a **3**-MMNP system. The interfacial **1**-MMNP assembly remains stable with the extensive extraction of water by ethyl ether (Figure S3 of the Supporting Information). The continued extraction eventually leads to the formation of tiny droplets of **1**-MMNP assembly that lack fluidity, indicating the removal of the majority, if not all, of water. However, even after this process, fusion among AuNPs does not occur because of the effective steric protection of **1**, as evidenced by the ready dissolution of **1**-MMNP in water.

3.2. Particle Diameter and Solvent Dependence of Interfacial Assembly. The energy gain from the particle confinement is also proportional to the particle diameter, and therefore, the assembly is less stable for smaller-sized particles. Below a size threshold, thermal energy is sufficient enough to drive the displacement of particles from the interface. Indeed, variation of the AuNP core sizes in **1**-MMNPs indicates that the interfacial confinement is absent for AuNPs of 4.4 nm in diameter (Figure S4A of the Supporting Information). At this size regime, the lack of interfacial confinement is also supported by the contact angle measurement, where substantial deviation from 90° is observed (water/ether/**1**-MMNP contact angle: 70°).[11] Ligand surface coverage is not the key determinant of MMNP partitioning efficacy at the interface, as confirmed on MMNPs with varied adsorbate functionalization times (1, 5, and 24 h). Similar close-packed structures were observed at the liquid−liquid interface for **1**-MMNPs of 26 and 60 nm AuNP core sizes (Figure S5 of the Supporting Information). Toluene, ethyl acetate, and chloroform could also support the formation of an interfacial film from aqueous-dispersed **1**-MMNPs (Figure S4B of the Supporting Information). However, ICP-AES characterization indicates that the majority of **1**-MMNPs resides in the aqueous phase (e.g., 82% for the toluene case).

4. Solvent-Dependent Dispersion State of MMNPs in a Homogeneous Solvent Mixture. The generation of interfacial assembly from MMNPs involves the use of a solvent mixture with constituent phases segregated. To gain access to MMNP-assembled constructs beyond the interfacial confinement regime, a homogeneously mixed solvent mixture has to be used. Although aqueous solution of **1**-MMNPs could be homogeneously suspended in a plethora of solvents, they appear distinctly different in different solvents. Divergent dispersion pathways would ensue after the mixing of aqueous **1**-MMNPs and an organic solvent. In this homogeneous solvent phase regime, one can imagine that the interfacial energies of the water/organic interface, MMNP/water interface, ligand phase/water interface, MMNP/organic interface, and ligand phase/organic interface dictate the final MMNP dispersion state. The ligand phase/water interfacial energy is relatively low so that the ligand can be fully solvated with water, possesses an extended conformation, provides steric protection for MMNPs, and leads to the individually dispersed state of MMNPs in the original aqueous solution. MMNPs will retain the individually dispersed state, and the solution will appear red (ethanol, *n*-propanol, *sec*-propanol, ethylene glycol, glycerol) (Figure S6A of the Supporting Information) if (1) water/organic interfacial energy is approaching zero as in the completely miscible case and (2) ligand phase/organic interfacial energy is also relatively low as MMNPs could be freely dissolved in the organic phase (the ligand shell is in the extended conformation and can provide steric protection[12]). MMNPs will be aggregated into random networked structures, and the solution will appear blue/purple (methanol, *t*-butanol, THF, ethyleneglycol dimethyl ether) (Figure S6B of the Supporting Information) if (1) water/organic interfacial energy is approaching zero as in the completely miscible case and (2) ligand phase/organic interfacial energy is relatively high as MMNPs could not be freely dissolved in the organic phase (the ligand shell is in the collapsed conformation and cannot provide steric protection[12]). MMNPs will be aggregated into well-defined discrete ensembles (*n*-butanol, *n*-hexanol, *n*-octanol) (Figure 3, Figures S7 and S8 of the Supporting Information) if (1) water/organic interfacial energy is positive (effective interfacial energy[13]) as in the partially miscible case and (2) the proper three (water/organic, MMNP/water, MMNP/organic) interfacial energy values lead to the confinement of MMNPs either in the aqueous phase or at the water/organic interface. The effective interfacial energy provides the necessary water/organic interfacial boundary to allow the formation of regularly shaped MMNP ensemble architecture in an orderly fashion through the proper flow of liquid phases. A better-structured assembly could be achieved through the initial interfacial assembly of MMNPs that enables the improved control of MMNP packing process.

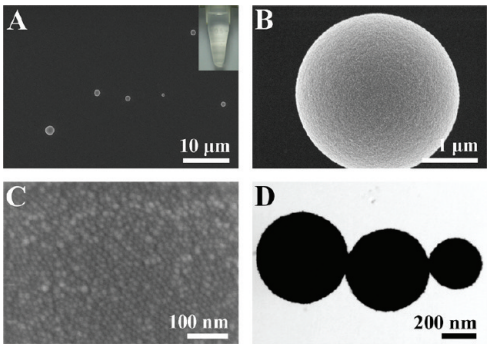

Figure 3. Formation of **1**-MMNP-assembled spherical ensemble structure in the mixture of water and *n*-butanol. (A−C) SEM and (D) transmission electron microscopy (TEM) micrographs at different magnifications of **1**-MMNP-assembled, spherical structure generated by mixing 60 μL aqueous solution of 13 nm **1**-MMNPs and 1 mL *n*-butanol. The inset in A displays the macroscopic image of the colorless solution. The solution turned colorless because of the formation of MMNP-assembled ensemble structure.

5. Self-Assembly of MMNPs into Spherical Construct and Optical Property. As mentioned above, the interactions among all the solution components dictate the final dispersion state of MMNPs. The diffusion of water into *n*-butanol, facilitated by violent shaking, allows the formation of spherical assembly of **1**-MMNPs (Figure 3). The extraordinary efficacy attested by the methodology is derived from a unique combination of and therefore a distinct driving force from the solvent partitioning and molecular interactions, in contrast to the long assembly time frame typically observed thus far.[7a] Key to the formation of spherical assembly is the existence of densely packed, interfacially confined **1**-MMNPs, which impart a hardening effect (Marangoni effect)[14] on the dispersed aqueous phase and which allow for the orderly flow of solvent from globularly shaped droplets. The extinction spectrum of spherical assembly exhibits a broad band centered at 583 nm (Figure S9 of the Supporting Information), reflecting the plasmonic coupling of individual **1**-MMNPs. Reaction in an alcoholic solvent of longer chain length does not affect the nature of the assembly process. For example, spherical assembly of **1**-MMNPs occurs in both *n*-hexanol and *n*-octanol (Figures S7 and S8 of the Supporting Information). An exquisitely controlled capsule structure comprising microspheres has been

generated through an emulsification sphere adsorption cross-linking phase-transfer procedure,[15] allowing the fabrication of colloidosome with selective permeability. In addition, the dense packing of microspheres into regularly shaped clusters through the emulsion process has been elegantly demonstrated by the Pine group.[16] Fluid removal from the droplets leads to the polyhedral arrangement of colloidal entities. To prove the hypothesis that initial interfacial confinement of MMNPs is the prerequisite for the formation of well-defined discrete ensemble structures, the behavior of an MMNP system in the solvent phase-segregated regime has been examined. Indeed, self-assembly has been observed for **1**-MMNPs at the *n*-butanol/water interface under phase-segregated static conditions (Figure S10 of the Supporting Information). In contrast, the lack of interfacial confinement capability from **2**-MMNPs results in extensive indentation in their spherical ensemble construct (Figures S11 and S12 of the Supporting Information).

5.1. Structural Characterization of MMNP Spherical Assembly. The spherical **1**-MMNP assembly generated in the water/*n*-butanol mixture provides an intriguing example of how to expeditiously fabricate a complex system in the fluid phase. Dynamic light scattering (DLS) supports the formation of self-assembled structure in the solution state (Figure S13 of the Supporting Information). Compared with SEM, the smaller size measured by DLS is attributed to the faster sedimentation speed of larger-sized spherical assembly. To probe the internal structure of the spherical assembly, focused ion beam (FIB) was used as a micromachining tool to sputter away part of the specimen. The cross section image revealed the presence of a solid core comprising tightly packed **1**-MMNPs (Figure S14A−C of the Supporting Information). However, because of the damaging effect exerted by the FIB processing, the structure of the outmost surface was destructed. A nondamaging acid breakage method could be employed to reveal the true spatial arrangement of MMNPs (vide infra). The internal stress generated through the strengthened hydrogen bonding interactions upon carboxylic acid protonation triggers the cracking of the spherical assembly. Alternatively, synchrotron small-angle X-ray scattering (SAXS) experiment could be used to probe the internal structure in reciprocal space. Significantly, the scattering pattern indicates the massive dominance of well-defined and ordered structure (Figure S14D of the Supporting Information). This crystalline packing indeed manifests the high efficacy of fluid phase in the establishment of a dynamic setting for achieving the optimum organized structure.

The introduction of an additional solvent component allows one to fine-tune the morphology of the assembled structure. In this regard, ethyl ether could be used for the generation of a spherical structure with highly ordered arrangement of **1**-MMNPs in the presence of a larger amount of water (Figure S15 of the Supporting Information). The order of the spherical assembly could be visualized through the acid breakage method, and remarkably, crystalline packing of **1**-MMNPs could be observed all over the exposed surface (Figure S16A, B of the Supporting Information). The periodic placement of **1**-MMNPs is again supported by synchrotron SAXS measurement in reciprocal space (Figure S16C of the Supporting Information), where prominent peaks indicate the structural ordering in the assembled material.

5.2. Stability of MMNP Spherical Assembly. The spherical assembly is stable against ultrasonication and heating, suggesting the presence of a strong cohesive force. However, if one puts the isolated spherical assembly structure into pure water, dissolution of **1**-MMNPs readily occurs in a rapid and violent fashion, suggesting its high-energy state in this solvent medium. One can also switch the assembled structure into individually dispersed **1**-MMNPs in water through phase separation as generated by the addition of water into the colorless mixture. By virtue of its large size, the assembled structure will settle down at the bottom of the vial upon prolonged standing (Figure S17 of the Supporting Information), albeit with morphology unaltered.

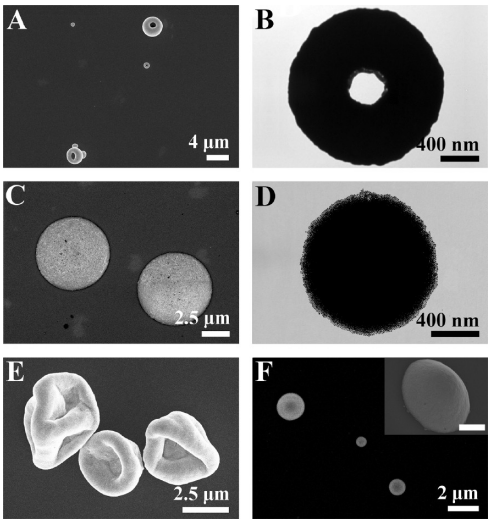

Figure 4. Generation of distinct **1**-MMNP-assembled structures under different conditions. (A) SEM and (B) TEM micrographs of torus-shaped structure (25 μL aqueous solution of 13 nm **1**-MMNPs, 500 μL *n*-butanol, and 500 μL ethyl ether). (C) SEM and (D) TEM micrographs of disk-shaped structure (52 μL aqueous solution of 13 nm **1**-MMNPs, 8 μL aqueous solution of 0.5 M 2,2′-(ethylenedioxy)bis-(ethylamine), and 1 mL *n*-butanol). The proton on **1**-MMNPs was first transformed into an ammonium salt through initial overnight reaction of **1**-MMNPs with an ammonia solution. (E) SEM micrograph of collapsed capsule structure (58 μL aqueous solution of 13 nm **1**-MMNPs, 2 μL aqueous solution of 0.1 M NaOH, and 1 mL *n*-butanol). (F) SEM micrograph of truncated spherical structure (58 μL aqueous solution of 13 nm **1**-MMNPs, 2 μL aqueous solution of 0.1 M NaOH, and 1 mL *n*-butanol at 17 °C). The inset in F displays the image of the structure at a tilted angle (scale bar: 1 μm). The truncated spherical structure is most likely formed on the solid substrate. The original ensemble structure in the solution state is conjectured to be a flattened sphere.

5.3. Effect of Agitation, Mixing, and Stirring on the MMNP Assembly Process. The formation of MMNP spherical assembly relies on the proper transfer of solvents across the initial interfacial boundary of the two fluid phases, where MMNPs are confined. The extent of agitation, mixing, and stirring will dictate the flow dynamics and therefore the final ensemble structures created. Several modes of perturbation were employed to examine the effects of these experimental variables on the assembly process. To gain insight into the impact of agitation, low to medium mechanical force was afforded through an orbital shaking incubator. Indeed, this mode of perturbation allows the observation of ensemble structural evolution, depending on the shaking speed, from planar agglomerate first to curved aggregate, then to giant hollow sphere, and finally, to small compact sphere (Figure S18 of the Supporting Information). This structural variation is most likely reflecting the difference in the diffusion rate of the fluid phase under different agitation conditions, which

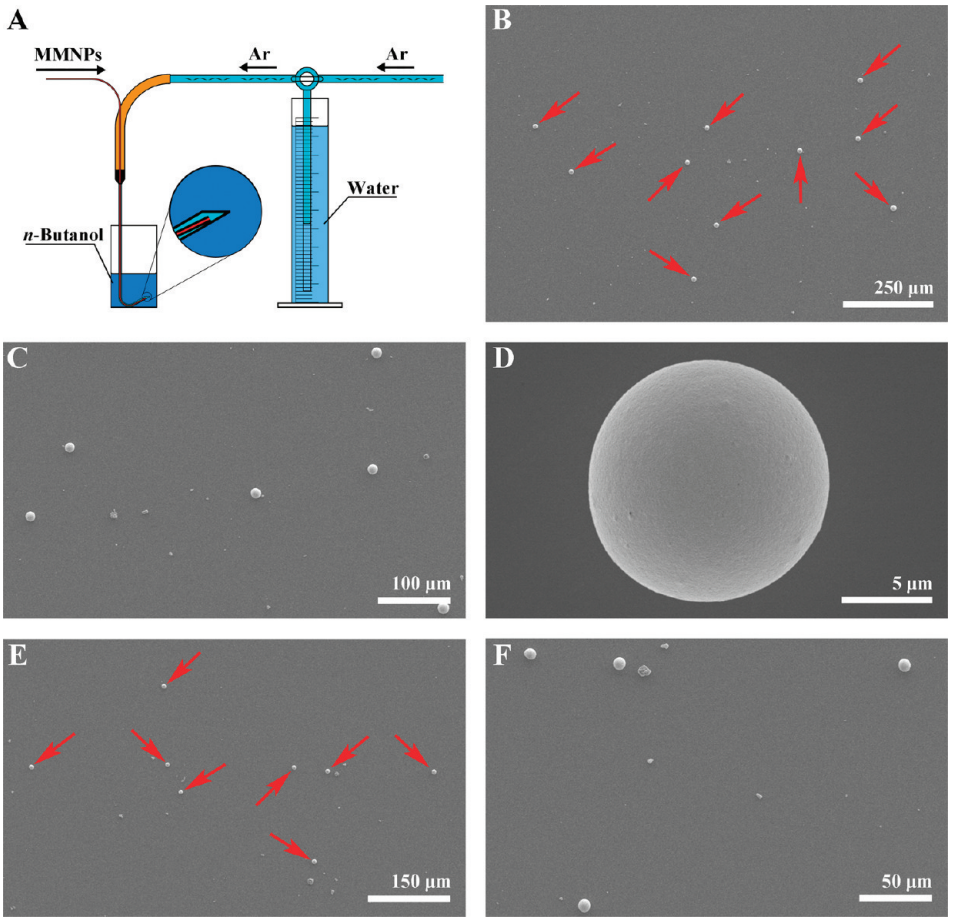

Figure 5. Monodispersity and size control of **1**-MMNP-assembled spherical ensemble structure through a microfluidics method. (A) Schematic illustration of the microfluidics setup. Argon gas with a desired pressure is used to carry a uniform volume of aqueous-dispersed MMNPs into *n*-butanol and to provide the requisite perturbation force for the generation of spherical ensemble structure. MMNPs are flown at a microinjection pump-controlled speed through a capillary tube (with outer and inner diameters of 365 and 25 μm, respectively). Argon gas is flown through a 600 μm diameter needle surrounding the capillary tube at a controlled pressure. (B−D) SEM micrographs at different magnifications of **1**-MMNP-assembled, uniform-sized spherical structure (14.3 $\pm$ 0.4 μm) generated by injecting, at a speed of 0.67 μL/min, 60 μL aqueous solution of 13 nm **1**-MMNPs into 50 mL *n*-butanol under the flow of argon gas (needle tip depth: 31 mm; argon pressure: 85 mm). (E, F) SEM micrographs at different magnifications of **1**-MMNP-assembled, uniform-sized spherical structure (9.1 $\pm$ 0.4 μm) generated by injecting, at a speed of 0.67 μL/min, 60 μL aqueous solution of 13 nm **1**-MMNPs into 50 mL *n*-butanol under the flow of argon gas (needle tip depth: 31 mm; argon pressure: 102 mm). For clarification, the spherical ensemble structure in B and E has been designated with a red arrow.

will in turn influence the packing characteristic of MMNPs. Vortexing is a foremost tool to provide efficient mixing through the turbulent flow of fluid. Under the mixing settings employed herein, MMNP spherical assembly invariably was generated regardless of the vortexing time period (Figure S19 of the Supporting Information). Stirring provides another channel to accelerate the mass transfer of chemical ingredients. However, it is not as effective as vortexing for the phase homogenization. As a result, no spherical assembly could be observed even at a relatively high stirring speed (Figure S20 of the Supporting Information). The above experiments demonstrate the profound importance of a highly effective mixing scheme for the synthesis of well-defined MMNP spherical assemblies.

6. Diversified Self-Assembly Pathways for MMNPs in Homogeneous Solvent Mixtures. We hypothesized that a ternary solvent system could provide the possibility of reversing the Marangoni effect through the instant creation of local interfacial regions with low energies, thus causing fast thinning and collapse of the interfacial lamella and breakup of the droplets (like the defoaming process). Indeed, the addition of ethyl ether is effective for the production of a torus-shaped, empty ring **1**-MMNP ensemble structure in the presence of a smaller amount of water (Figure 4A, B). As the interfacial residence probability of **1**-MMNPs and the corresponding deformability of the dispersed droplets can be tuned through a change in ionization state, it would be interesting to see if such an alteration would lead to a distinct morphology of the assembly structure. Interestingly, one can modulate the assembly process through the transformation of **1**-MMNP ligand shell into an ammonium salt and the addition of a reagent that could interact with the transformed **1**-MMNPs. Thus, the addition of 2,2′-(ethylenedioxy)bis(ethylamine) directs the assembly pathway toward the densely packed, disk-shaped morphology (Figure 4C, D and Figure S21 of the Supporting Information), enabled by the orderly flow of solvent across the tight, cross-linked **1**-MMNP layer within the highly deformable droplets. The addition of NaOH could likewise cause a lesser degree of interfacial confinement for **1**-MMNPs through the creation of charge repulsion. Furthermore, the accelerated solvent flow dynamics due to the existence of a leaky interface

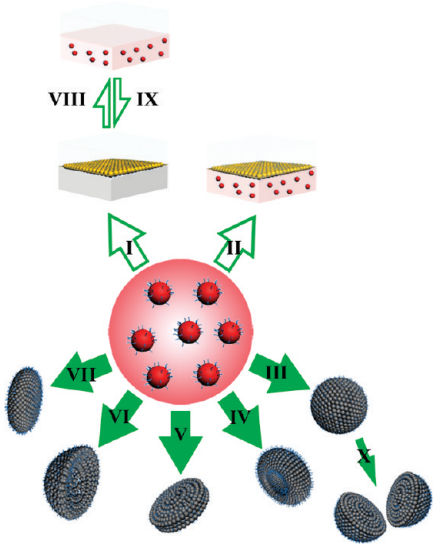

Figure 6. Schematic representation of the diversified assembly pathways with **1**-MMNPs. MMNP thin film formation at the interface of water and ethyl ether (**I**, the aqueous phase is completely deprived of MMNPs) and at the interface of water and toluene or ethyl acetate (**II**, the aqueous phase is filled with red-colored MMNPs; for chloroform, the aqueous phase is at the top). **III**: MMNP spherical ensemble structure formation in the solvent mixture of water and *n*-butanol. **IV**: MMNP torus-shaped ensemble structure formation in the solvent mixture of water, *n*-butanol, and ethyl ether. **V**: MMNP disk-shaped ensemble structure formation in the solvent mixture of water and *n*-butanol with the addition of 2,2′-(ethylenedioxy)bis(ethylamine). **VI**: MMNP collapsed capsule ensemble structure formation in the solvent mixture of water and *n*-butanol with the addition of NaOH. **VII**: MMNP flattened spherical ensemble structure formation in the solvent mixture of water and *n*-butanol with the addition of NaOH at lower temperature. Redispersion of MMNPs at the interface back into the aqueous phase through the addition of NaOH (**VIII**) and reformation of MMNP thin film through the addition of HCl into **VIII** (**IX**). **X**: Breakage of MMNP spherical ensemble structure into half-spherical parts through the addition of HCl. Spherical building blocks (red, golden, and gray in color): AuNP cores of MMNPs. Blue curved lines on the spherical building blocks: monolayer molecules. Green arrows: fabrication of ensemble constructs from MMNPs and further transformation of the constructs.

does not permit the formation of solidly packed **1**-MMNP assembly structure. Indeed, with an increased amount of base, one can see the transition of the ensemble construct from a perfect sphere to a collapsed capsule (Figure 4E, Figures S22 and S23 of the Supporting Information). The thickness of the capsule wall is also dependent on the amount of base added, reflecting more pronounced charge repulsion among deprotonated carboxylic acid at higher base concentrations (Figures S24 and S25 of the Supporting Information). It is not exactly known whether the hollow capsule is collapsed in the solution or in the solvent-dried state at this point. If the base is added to the solution mixture after the formation of spherical assembly, no major change could be observed, suggesting the robustness of the assembled structure under this condition. The effect of charge repulsion on the NP-based assembly is further demonstrated with an oligonucleotide-modified AuNP system. Indeed, because of the high charge density associated with each individual AuNP, the assembled structure is a highly irregular-shaped capsule with pores all over the wall (Figure S26 of the Supporting Information). Since the physical properties of all the components are temperature-dependent, adjustments in temperature could be used for tuning the assembled structure. For example, a mixture of **1**-MMNPs, base, water, and *n*-butanol at a lower temperature, because of the slow solvent flow dynamics, leads to the formation of a densely packed, truncated sphere within the deformed droplets (Figure 4F and Figure S27 of the Supporting Information). The truncated spherical structure is most likely formed on the substrate because of the soft nature of the ensemble construct. The ensemble construct in the original solution state is speculated to be a flattened sphere. Taken together, diversified architectures have been assembled in the homogeneous solvent mixture, and the degree of Marangoni effect/droplet deformability and the solvent flow dynamics likely dictate the exact type of structure generated.

7. Control over Monodispersity and Size of MMNP Ensemble Constructs. Functional applications of a synthetic architecture generally require the access to uniformly distributed target objects. Key structural parameters, monodispersity and size of the MMNP ensemble constructs, should therefore be controlled if further exploitation of the assembly system is desired. We envisioned that a microinjection pump could be used to introduce a uniform volume of aqueous-dispersed MMNPs into the requisite fluid media at a regular time interval. However, as demonstrated above, the type of final ensemble construct fabricated is dictated by the solvent flow dynamics, which is in turn defined by the mode of mechanical perturbation. Through preliminarily designed, geometrically constrained microfluidics setup (Figure 5A),[17] we demonstrate that one can create spherical assembly structure with controlled monodispersity and size by employing gas bubble as the generator of perturbation force (Figure 5B−F). In addition and satisfyingly, the same type of apparatus can be readily extended to the preparation of all the other types of ensemble constructs with a uniform size distribution (Figure S28 of the Supporting Information).

Taken together, in contrast to the one-building-block-one-assembly-construct regime typically achieved thus far, the above data suggest that we can achieve diversified assembly on MMNPs through the control of such parameters as solvent, pH, affinity molecule, and temperature (Figure 6). The versatility of the method and the broad architecture scope signify the notion that MMNPs would arrange themselves in a way to maximize interactions among motifs with inherent affinities toward one another and simultaneously to minimize repulsive interactions. The exceedingly short period of assembly time provides the possibility of a rapid entry into the chemical synthesis of diversity. Incorporation of uniquely structured molecular synthons such as the one reported herein (**1**) into multisegmented nanoscale building blocks is expected to generate more complex self-organized architectures (e.g., hierarchical structures) that are otherwise impossible to obtain.

CONCLUSIONS

In conclusion, diversified assembly has been achieved on a designer MMNP system. The orchestrated organization of MMNPs within the confines of solvent media permits the formation of polymorphic ensemble constructs. These diversified modes of assembly complement the conventionally used, amphiphilicity-driven strategy. We anticipate that our straightforward and effective assembly methodology will inspire the establishment of new synthetic paradigms for the creation of future-generation ordered matter.

EXPERIMENTAL SECTION

General Methods. All chemicals were obtained from commercial source and were used without further purification unless otherwise noted. $HAuCl_4 \cdot 4H_2O$ (99%) was purchased from Shanghai Chemical Reagent Co. Ltd. Trisodium citrate (98%) and ethyl ether (anhydrous) were purchased from Sinopharm Chemical Reagent Co. Ltd. Acetic acid and 2,2′-(ethylenedioxy)-bis(ethylamine) (97+%) were purchased from Alfa Aesar. Methanol, toluene, ethyl acetate, trichloromethane, ammonia solution (25%), and sodium hydroxide (NaOH) were from Nanjing Chemical Reagent Co. Ltd. *n*-Butanol (AR) was from Shanghai Shenbo Chemical Co. Ltd. *sec*-Butanol (AR) was from Shanghai Lingfeng Chemical Reagent Co. Ltd. Petroleum ether was from Beijing Changhai Chemical Co. Ltd. Silicon wafer was from KMT Co. Ltd. The synthesis of molecule **1** has been reported previously.[9]

Nanopure water (18.2 MΩ·cm), purified by Sartorius Arium 611 system, was used throughout the experiment. All glassware was cleaned using aqua regia solution ($HCl:HNO_3$ = 3:1, v/v) and subsequently was rinsed with a copious amount of nanopure water. Centrifugation of AuNPs was achieved on a Sigma laboratory centrifuge. Centrifugal filter device (Millipore, 30 kD cutoff) was used for the preparation of 4.4 nm AuNPs. Carbon film-coated copper TEM grids (230 mesh) were purchased from Beijing Zhongjingkeyi Technology Co. Ltd.

Measurements. TEM was performed on a JEOL 2000FX machine operating at an acceleration voltage of 120 kV. The sample was prepared by drop-casting a AuNP solution onto a carbon-coated copper grid and by allowing the solvent to evaporate. SEM was performed on a Hitachi S-4800 machine operating at an acceleration voltage of 10 kV. Atomic force microscopy (AFM) was performed on a Veeco Multimode V facility. The sample was prepared by drop-casting a AuNP solution onto a silicon wafer and by draining away the excess solvent with a filter paper. The contact angle was measured by a CAM 200 optical contact angle meter produced by KSV Instrument Ltd. FIB processing was achieved on an FEI STRATA FIB 201 facility.

Preparation of AuNPs. AuNPs of approximately 13 nm in diameter were prepared by the citrate reduction of $HAuCl_4$.[18] An aqueous solution of $HAuCl_4$ (1 mM, 500 mL) was brought to a reflux while stirring, and then 50 mL of a 38.8 mM trisodium citrate solution was added quickly, which resulted in a change in the solution color from pale yellow to deep red. After the color change, the solution was refluxed for an additional 1 h and then was allowed to cool to room temperature. Other-sized gold NPs were prepared by adjusting the amount of reducing agent of sodium citrate (26 nm: 25 mL; 60 nm: 15 mL).[18]

Preparation of 1-MMNPs. A 35 μL aqueous solution of **1** (~10 mM) was added into 1 mL freshly prepared AuNPs (13, 26, or 60 nm). The modification was allowed to proceed at room temperature for 24 h. Excess molecule **1** was removed by three cycles of centrifugation (15 000 rpm, 15 min, 4 °C)/washing (with water)/redispersion. **1**-MMNPs were obtained by suspending the precipitate in water (e.g., 60 μL).

For AuNPs of 4.4 nm, **1**-MMNPs were prepared according to the literature.[9] $HAuCl_4 \cdot 4H_2O$ (411.85 mg, 1 mmol) and **1** (134 mg, 0.5 mmol) were dissolved in a mixture of 60 mL methanol and 10 mL acetic acid. Upon vigorous stirring, 30 mL of an ice-cold 0.5 M aqueous solution of $NaBH_4$ was added within a few minutes. The reaction mixture changed color immediately from yellow-greenish to dark brown. The AuNPs prepared after this step were soluble in water. The AuNP solution was transferred into a centrifugal filter device (30 kD cutoff) and was purified by four cycles of centrifugation (3500 rpm, 15 min, 4 °C)/washing (with water)/redispersion. The final volume of water for suspending **1**-MMNPs of 4.4 nm was approximately 20 mL. The **1**-MMNP solution was put in a glass bottle and was stored at 4 °C before use.

Preparation of Oligonucleotide-Modified AuNPs. The preparation of oligonucleotide-modified AuNPs was accomplished according to the literature protocol.[19] The sequence of the oligonucleotide used for the modification is 5′ HS-TTTCTT-TTATCCTTATCAAT 3′.

ASSOCIATED CONTENT

Supporting Information. Data on the characterization and assembly of **1**-MMNPs. This material is available free of charge via the Internet at http://pubs.acs.org.

AUTHOR INFORMATION

Corresponding Author
*E-mail: jinz@nju.edu.cn.

ACKNOWLEDGMENT

J.Z. acknowledges support from the National Science Foundation of China (20974044, 90923006) and the National Basic Research Program of China (2007CB925103, 2011CB935801).

REFERENCES

(1) Whitesides, G. M.; Grzybowski, B. *Science* **2002**, *295*, 2418–2421.

(2) Piner, R. D.; Zhu, J.; Xu, F.; Hong, S.; Mirkin, C. A. *Science* **1999**, *283*, 661–663.

(3) (a) Ouyang, M.; Awschalom, D. D. *Science* **2003**, *301*, 1074–1078. (b) Courty, A.; Mermet, A.; Albouy, P. A.; Duval, E.; Pileni, M. P. *Nat. Mater.* **2005**, *4*, 395–398. (c) Didiot, C.; Pons, S.; Kierren, B.; Fagot-Revurat, Y.; Malterre, D. *Nat. Nanotechnol.* **2007**, *2*, 617–621. (d) Klajn, R.; Bishop, K. J. M.; Fialkowski, M.; Paszewski, M.; Campbell, C. J.; Gray, T. P.; Grzybowski, B. A. *Science* **2007**, *316*, 261–264. (e) Urban, J. J.; Talapin, D. V.; Shevchenko, E. V.; Kagan, C. R.; Murray, C. B. *Nat. Mater.* **2007**, *6*, 115–121.

(4) Bishop, K. J. M.; Wilmer, C. E.; Soh, S.; Grzybowski, B. A. *Small* **2009**, *5*, 1600–1630.

(5) (a) Zhou, X.; Cao, P.; Tian, Y.; Zhu, J. *J. Am. Chem. Soc.* **2010**, *132*, 4161–4168. (b) Zhou, X.; Xia, S.; Lu, Z.; Tian, Y.; Yan, Y.; Zhu, J. *J. Am. Chem. Soc.* **2010**, *132*, 6932–6934. (c) Qiu, F.; Jiang, D.; Ding, Y.; Zhu, J.; Huang, L. L. *Angew. Chem., Int. Ed.* **2008**, *47*, 5009–5012. (d) Hong, M.; Zhou, X.; Lu, Z.; Zhu, J. *Angew. Chem., Int. Ed.* **2009**, *48*, 9503–9506.

(6) Love, J. C.; Estroff, L. A.; Kriebel, J. K.; Nuzzo, R. G.; Whitesides, G. M. *Chem. Rev.* **2005**, *105*, 1103–1169.

(7) (a) Boal, A. K.; Ilhan, F.; Derouchey, J. E.; Thurn-Albrecht, T.; Russell, T. P.; Rotello, V. M. *Nature* **2000**, *404*, 746–748. (b) Zubarev, E. R.; Xu, J.; Sayyad, A.; Gibson, J. D. *J. Am. Chem. Soc.* **2006**, *128*, 15098–15099. (c) Lin, Y.; Skaff, H.; Emrick, T.; Dinsmore, A. D.; Russell, T. P. *Science* **2003**, *299*, 226–229. (d) Duan, H.; Wang, D.; Kurth, D. G.; Möhwald, H. *Angew. Chem., Int. Ed.* **2004**, *43*, 5639–5642. (e) Harrison, R. G.; Washburn, A. L.; Pickett, A. T.; Call, D. M. *J. Mater. Chem.* **2008**, *18*, 3718–3722.

(8) (a) Lee, M.; Cho, B.-K.; Zin, W.-C. *Chem. Rev.* **2001**, *101*, 3869–3892 and references therein. (b) Cui, H.; Chen, Z.; Zhong, S.; Wooley, K. L.; Pochan, D. J. *Science* **2007**, *317*, 647–650. (c) Gädt, T.; Leong, N. Z.; Cambridge, G.; Winnik, M. A.; Manners, I. *Nat. Mater.* **2009**, *8*, 144–150.

(9) Lu, Z.; Shu, X.; Zhang, K.; Zhu, J. *J. Phys. Chem. C* **2009**, *113*, 12950–12953.
(10) Huang, D. M.; Chandler, D. *Proc. Natl. Acad. Sci. U.S.A.* **2000**, *97*, 8324–8327.
(11) (a) Binks, B. P.; Lumsdon, S. O. *Phys. Chem. Chem. Phys.* **2000**, *2*, 2959–2967. (b) Binks, B. P.; Lumsdon, S. O. *Langmuir* **2001**, *17*, 4540–4547. (c) Binks, B. P.; Clint, J. H. *Langmuir* **2002**, *18*, 1270–1273. (d) Binks, B. P. *Curr. Opin. Colloid Interface Sci.* **2002**, *7*, 21–41. (e) Binks, B. P.; Rodrigues, J. A. *Langmuir* **2003**, *19*, 4905–4912. (f) Binks, B. P.; Whitby, C. P. *Langmuir* **2004**, *20*, 1130–1137. (g) Horozov, T. S.; Binks, B. P. *Angew. Chem., Int. Ed.* **2006**, *45*, 773–776. (h) Binks, B. P. *Phys. Chem. Chem. Phys.* **2007**, *9*, 6298–6299. (i) Binks, B. P.; Liu, W.; Rodrigues, J. A. *Langmuir* **2008**, *24*, 4443–4446. (j) Stocco, A.; Drenckhan, W.; Rio, E.; Langevin, D.; Binks, B. P. *Soft Matter* **2009**, *5*, 2215–2222. (k) Binks, B. P.; Fletcher, P. D. I.; Holt, B. L.; Kuc, O.; Beaussoubre, P.; Wong, K. *Phys. Chem. Chem. Phys.* **2010**, *12*, 2219–2226. (l) Binks, B. P.; Rocher, A. *Phys. Chem. Chem. Phys.* **2010**, *12*, 9169–9171.
(12) (a) Sheiko, S. S.; Möller, M. *Chem. Rev.* **2001**, *101*, 4099–4123. (b) Barbey, R.; Lavanant, L.; Paripovic, D.; Schüwer, N.; Sugnaux, C.; Tugulu, S.; Klok, H.-A. *Chem. Rev.* **2009**, *109*, 5437–5527.
(13) Pojman, J. A.; Whitmore, C.; Liveri, M. L. T.; Lombardo, R.; Marszalek, J.; Parker, R.; Zoltowski, B. *Langmuir* **2006**, *22*, 2569–2577.
(14) (a) Davidson, M. R.; Harvie, D. J. E. *ANZIAM J.* **2007**, *48*, C661–C676. (b) Bazhlekov, I. B.; Anderson, P. D.; Meijer, H. E. H. *J. Colloid Interface Sci.* **2006**, *298*, 369–394. (c) Vlahovska, P. M.; Loewenberg, M.; Blawzdziewicz, J. *Phys. Fluids* **2005**, *17*, 103103. (d) Usta, O. B.; Perchak, D.; Clarke, A.; Yeomans, J. M.; Balazs, A. C. *J. Chem. Phys.* **2009**, *130*, 234905.
(15) (a) Dinsmore, A. D.; Hsu, M. F.; Nikolaides, M. G.; Marquez, M.; Bausch, A. R.; Weitz, D. A. *Science* **2002**, *298*, 1006–1009. (b) Lawrence, D. B.; Cai, T.; Hu, Z.; Marquez, M.; Dinsmore, A. D. *Langmuir* **2007**, *23*, 395–398. (c) Zeng, C.; Bissig, H.; Dinsmore, A. D. *Solid State Commun.* **2006**, *139*, 547–556. (d) Hsu, M. F.; Nikolaides, M. G.; Dinsmore, A. D.; Bausch, A. R.; Gordon, V. D.; Chen, X.; Hutchinson, J. W.; Weitz, D. A.; Marquez, M. *Langmuir* **2005**, *21*, 2963–2970. (e) Lin, Y.; Böker, A.; Skaff, H.; Cookson, D.; Dinsmore, A. D.; Emrick, T.; Russell, T. P. *Langmuir* **2005**, *21*, 191–194. (f) Böker, A.; Lin, Y.; Chiapperini, K.; Horowitz, R.; Thompson, M.; Carreon, V.; Xu, T.; Abetz, C.; Skaff, H.; Dinsmore, A. D.; Emrick, T.; Russell, T. P. *Nat. Mater.* **2004**, *3*, 302–306. (g) Shah, R. K.; Kim, J.-W.; Weitz, D. A. *Langmuir* **2010**, *26*, 1561–1565. (h) Böker, A.; He, J.; Emrick, T.; Russell, T. P. *Soft Matter* **2007**, *3*, 1231–1248. (i) Lee, D.; Weitz, D. A. *Adv. Mater.* **2008**, *20*, 3498–3503. (j) Studart, A. R.; Shum, H. C.; Weitz, D. A. *J. Phys. Chem. B* **2009**, *3*, 3914–3919. (k) Kim, J.-W.; Fernández-Nieves, A.; Dan, N.; Utada, A. S.; Marquez, M.; Weitz, D. A. *Nano Lett.* **2007**, *7*, 2876–2880.
(16) (a) Yi, G.-R.; Manoharan, V. N.; Klein, S.; Brzezinska, K. R.; Pine, D. J.; Lange, F. F.; Yang, S.-M. *Adv. Mater.* **2002**, *14*, 1137–1140. (b) Manoharan, V. N.; Elsesser, M. T.; Pine, D. J. *Science* **2003**, *301*, 483–487. (c) Yi, G.-R.; Thorsen, T.; Manoharan, V. N.; Hwang, M.-J.; Jeon, S.-J.; Pine, D. J.; Quake, S. R.; Yang, S.-M. *Adv. Mater.* **2003**, *15*, 1300–1304. (d) Manoharan, V. N.; Pine, D. J. *MRS Bull.* **2004**, *29*, 91–95. (e) Yi, G.-R.; Manoharan, V. N.; Michel, E.; Elsesser, M. T.; Yang, S.-M.; Pine, D. J. *Adv. Mater.* **2004**, *16*, 1204–1208. (f) Cho, Y.-S.; Yi, G.-R.; Kim, S.-H.; Pine, D. J.; Yang, S.-M. *Chem. Mater.* **2005**, *17*, 5006–5013. (g) Cho, Y.-S.; Yi, G.-R.; Lim, J.-M.; Kim, S.-H.; Manoharan, V. N.; Pine, D. J.; Yang, S.-M. *J. Am. Chem. Soc.* **2005**, *127*, 15968–15975. (h) Zerrouki, D.; Rotenberg, B.; Abramson, S.; Baudry, J.; Goubault, C.; Leal-Calderon, F.; Pine, D. J.; Bibette, J. *Langmuir* **2006**, *22*, 57–62. (i) Kim, S.-H.; Lee, S. Y.; Yi, G.-R.; Pine, D. J.; Yang, S.-M. *J. Am. Chem. Soc.* **2006**, *128*, 10897–10904. (j) Yu, H.-K.; Yi, G.-R.; Kang, J.-H.; Cho, Y.-S.; Manoharan, V. N.; Pine, D. J.; Yang, S.-M. *Chem. Mater.* **2008**, *20*, 2704–2710.
(17) (a) Whitesides, G. M. *Nature* **2006**, *442*, 368–373. (b) Xu, S.; Nie, Z.; Seo, M.; Lewis, P.; Kumacheva, E.; Stone, H. A.; Garstecki, P.; Weibel, D. B.; Gitlin, I.; Whitesides, G. M. *Angew. Chem., Int. Ed.* **2005**, *44*, 724–728. (c) Dendukuri, D.; Pregibon, D. C.; Collins, J.; Hatton, T. A.; Doyle, P. S. *Nat. Mater.* **2006**, *5*, 365–369. (d) Anna, S. L.; Bontoux, N.; Stone, H. A. *Appl. Phys. Lett.* **2003**, *82*, 364–366.
(18) (a) Grabar, K. C.; Freeman, R. G.; Hommer, M. B.; Natan, M. J. *Anal. Chem.* **1995**, *67*, 735–743. (b) Mirkin, C. A.; Letsinger, R. L.; Mucic, R. C.; Storhoff, J. J. *Nature* **1996**, *382*, 607–609.
(19) Storhoff, J. J.; Elghanian, R.; Mucic, R. C.; Mirkin, C. A.; Letsinger, R. L. *J. Am. Chem. Soc.* **1998**, *120*, 1959–1964.